

Parametric dependent Hamiltonians, wave functions, random matrix theory, and quantal-classical correspondence

Doron Cohen¹ and Tsampikos Kottos²¹*Department of Physics, Harvard University, Cambridge, Massachusetts 02138*²*Max-Planck-Institut für Strömungsforschung, 37073 Göttingen, Germany*

(Received 22 September 2000; published 15 February 2001)

We study a classically chaotic system that is described by a Hamiltonian $\mathcal{H}(Q,P;x)$, where (Q,P) are the canonical coordinates of a particle in a two-dimensional well, and x is a parameter. By changing x we can deform the “shape” of the well. The quantum eigenstates of the system are $|n(x)\rangle$. We analyze numerically how the parametric kernel $P(n|m)=|\langle n(x)|m(x_0)\rangle|^2$ evolves as a function of $\delta x\equiv(x-x_0)$. This kernel, regarded as a function of $n-m$, characterizes the shape of the wave functions, and it also can be interpreted as the local density of states. The kernel $P(n|m)$ has a well-defined classical limit, and the study addresses the issue of quantum-classical correspondence. Both the perturbative and the nonperturbative regimes are explored. The limitations of the random matrix theory approach are demonstrated.

DOI: 10.1103/PhysRevE.63.036203

PACS number(s): 05.45.Mt, 03.65.Sq

I. INTRODUCTION

Consider a system whose total Hamiltonian is $\mathcal{H}(Q,P;x)$, where (Q,P) is a set of canonical coordinates and x is a constant parameter. This parameter may represent the effect of some externally controlled field. We assume that both $\mathcal{H}_0=\mathcal{H}(Q,P;x_0)$ and $\mathcal{H}=\mathcal{H}(Q,P;x)$ generate classically chaotic dynamics of similar nature. Moreover, we assume that $\delta x\equiv(x-x_0)$ is *classically small*, meaning that it is possible to apply linear analysis in order to describe how the energy surfaces $\mathcal{H}(Q,P;x)=E$ are deformed as a result of changing the value of x . Quantum mechanically, we can use a basis where $\mathcal{H}_0=\mathbf{E}_0$ has a diagonal representation, while

$$\mathcal{H}=\mathbf{E}_0+\delta x\mathbf{B}. \quad (1)$$

For reasonably small \hbar , it follows from general semiclassical considerations [1], that \mathbf{B} is a *banded matrix*. Generically, this matrix *looks random*, as if its off-diagonal elements were *independent* random numbers.

It was the idea of Wigner [2] 40 years ago, to study a simplified model, where the Hamiltonian is given by Eq. (1), and where \mathbf{B} is a *random banded matrix*. This is known as Wigner’s banded random matrix (WBRM) model. The applicability of such a model is a matter of *conjecture*. Obviously this conjecture should be tested.¹ The most direct way to test

it, which we are going to apply, is to take the matrix \mathbf{B} of a “physical” Hamiltonian, and then to randomize the signs of its off-diagonal elements. The outcome of such operation will be referred to as the *effective* WBRM model that is associated with the *physical* Hamiltonian. One issue of this paper is to make a comparison between the eigenstates of the physical Hamiltonian, and those of the associated effective WBRM model.

The *standard* WBRM model (unlike the “effective” one) involves an additional simplification. Namely, one assumes that \mathbf{B} has a rectangular band profile. The theory of eigenstates for the standard WBRM model is well known [2–4]. Increasing x , starting from $\delta x=0$, the eigenstates of Eq. (1) change their nature. The general questions to address are as follows.

(1) What are the *parametric regimes* in the parametric evolution of the eigenstates?

(2) How does the structure of the eigenstates change as we go through the subsequent regimes?

Recently some ideas have been introduced [5–7] how to go beyond Wigner’s theory in case of physical Hamiltonians. It has been suggested that there are at least three generic parametric scales $\delta x_c^{\text{qm}}\ll\delta x_{\text{prt}}\ll\delta x_{\text{SC}}$ that control the parametric evolution of the eigenstates. We shall define these parametric scales later. Accordingly one should distinguish between the standard perturbative regime ($\delta x\ll\delta x_c^{\text{qm}}$), the core-tail regime ($\delta x_c^{\text{qm}}\ll\delta x\ll\delta x_{\text{prt}}$), and the semiclassical regime ($\delta x\gg\delta x_{\text{SC}}$).

The purpose of this paper is not just to numerically establish (for the first time) the existence of the parametric regimes suggested in Refs. [5–7], but mainly to address question (2) above [8]. Namely, we would like to study how the structure of the eigenstates changes as we go through the subsequent regimes. In particular we would like to understand the significance of random matrix theory (RMT) assumptions in the general theoretical considerations. The latter issue has been left unexplored in the “quantum chaos” literature. (Note, however, that literally the same question is addressed in numerous publication once spectral statistics of eigenvalues, rather than eigenstate structure, is concerned.) We also suggest a procedure for “region analysis” of the eigenstate structure. We are going to distinguish between

¹To be more specific, one should be aware that there is a hierarchy of challenges where the applicability of the RMT approach should be tested. Namely, the study of spectral statistics, the study of eigenstates, and the study of quantum dynamics. In a previous work [11] we have argued that the RMT approach does not generally apply to the study of wave-packet dynamics, since it leads to a contradiction with the quantal-classical correspondence (QCC) principle. On the other hand, it is well known that spectral statistics are much more robust. In most of the RMT literature (including the later works by Wigner himself), it is assumed that for the purpose of quantum chaos studies, one can consider full (rather than banded) matrices, and the first term in Eq. (1) is generally neglected. In spite of these enormous simplifications, it turns out that the so-called Gaussian invariant ensembles (GOE, GUE) provide a valid description of some major spectral properties.

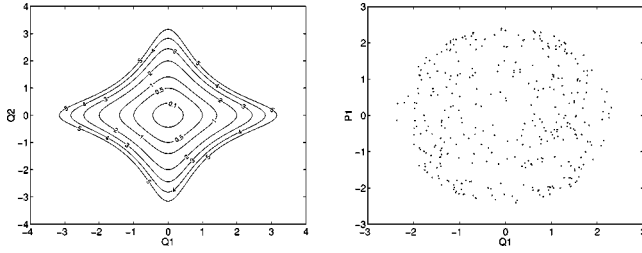


FIG. 1. *Left*: equipotential contours of the model Hamiltonian (2) with $x=x_0=1$. *Right*: A Poincaré section of a long trajectory ($0 < t < 1300$) that we have picked in order to get the fluctuating quantity $\mathcal{F}(t)$. The initial conditions are $(Q_1, Q_2, P_1, P_2) = (1, 0, 1, 2)$ corresponding to $E=3$. The trajectory is quite ergodic. It avoids some small quasiintegrable islands [the main one is around $(0, 0)$].

first-order tail regions (FOTR's), higher-order far-tail regions, and a nonperturbative (core) region. Our main conclusion is going to be that RMT is inadequate for the analysis of any features that go beyond first-order perturbation theory.

II. THE MODEL HAMILTONIAN

We study the Hamiltonian

$$\mathcal{H}(Q, P; x) = \frac{1}{2}(P_1^2 + P_2^2 + Q_1^2 + Q_2^2) + xQ_1^2Q_2^2 \quad (2)$$

with $x=x_0 + \delta x$ and $x_0=1$. This Hamiltonian describes the motion of a particle in a two-dimensional (2D) well (see Fig. 1). The units are chosen such that the mass is equal to one, the frequency for small oscillations is one, and for $\delta x=0$ the coefficient of the anharmonic term is also one. The energy E is the only dimensionless parameter of the classical motion. Our numerical study is focused on an energy window around $E \sim 3$ where the motion is mainly chaotic.

In the classical analysis there is only one parametric scale, which is $\delta x_c^{\text{cl}} \sim 1$. This scale determines the regime of (classical) linear analysis. For $\delta x \ll \delta x_c^{\text{cl}}$ the deformation of the energy surface $\mathcal{H}_0(Q, P; x) = E$ can be described as a linear process. Later we are going to give a precise mathematical formulation of this idea. From now on assume that we are in the classical linear regime.

Let us pick a very long ergodic trajectory $(Q(t), P(t))$ that covers densely the energy surface E . See Fig. 1. Let us define the fluctuating quantity

$$\mathcal{F}(t) \equiv -(\partial \mathcal{H} / \partial x) = -Q_1^2 Q_2^2. \quad (3)$$

For the later analysis it is important to know the distribution of the variable \mathcal{F} , and to characterize its temporal correlations. The average value is $F = \langle \mathcal{F} \rangle$. The angular brackets stand for microcanonical average over $(Q(0), P(0))$, which should be the same as time (t) average (due to the assumed ergodicity). The autocorrelation function of $\mathcal{F}(t)$ is

$$C(\tau) = \langle [\mathcal{F}(t) - F][\mathcal{F}(t + \tau) - F] \rangle. \quad (4)$$

Note that $C(\tau)$ is independent of t , and that the average over t should give the same result as a microcanonical average over $(Q(0), P(0))$.

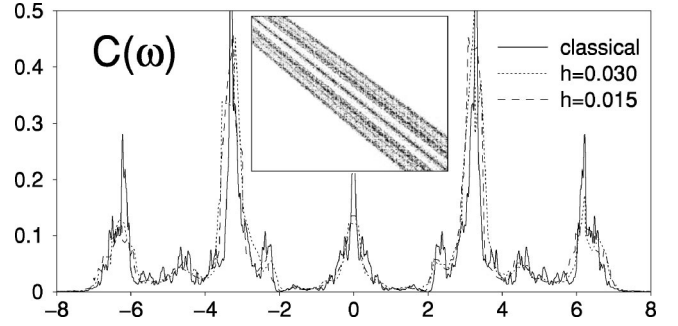


FIG. 2. The band profile $(2\pi\hbar/\Delta) \cdot |\mathbf{B}_{nm}|^2$ vs $\omega = (E_n - E_m)/\hbar$ is compared with the classical power spectrum $C(\omega)$. *Inset*: An image of a piece of the \mathbf{B} matrix.

The variance of the fluctuations is $C(0) = \langle (\mathcal{F} - F)^2 \rangle$. The correlation time will be denoted by τ_{cl} . Note that with our choice of units $\tau_{\text{cl}} \sim 1.0$, within the energy range of interest. The power spectrum $\tilde{C}(\omega)$ of the fluctuating $\mathcal{F}(t)$, is obtained via a Fourier transform of $C(\tau)$. See Fig. 2. The average F and the variance $C(0)$ determine just the first two moments of the \mathcal{F} distribution. The probability density of \mathcal{F} will be denoted by $P_{\mathcal{F}}(\mathcal{F})$.

All the required information for the subsequent semiclassical analysis is contained in the functions $C(\tau)$ and $P_{\mathcal{F}}(\mathcal{F})$ as defined above. All we have to do in order to numerically determine them is to generate one very long ergodic trajectory (see Fig. 1), to compute the respective $\mathcal{F}(t)$, and from it to extract the desired information (see Figs. 2 and 3). It is convenient to express $P_{\mathcal{F}}(\mathcal{F})$ in terms of a scaling function as follows:

$$P_{\mathcal{F}}(\mathcal{F}) = \frac{1}{\sqrt{C(0)}} \hat{P}_{\text{cl}} \left(-\frac{\mathcal{F} - F}{\sqrt{C(0)}} \right). \quad (5)$$

By this definition the scaled distribution $\hat{P}_{\text{cl}}(f)$ is characterized by a zero average ($\langle f \rangle = 0$), a unit variance ($\langle f^2 \rangle = 1$), and it is properly normalized. Note that $\hat{P}_{\text{cl}}(-f)$ rather than $\hat{P}_{\text{cl}}(f)$ corresponds to $P_{\mathcal{F}}(\mathcal{F})$. This has been done for later convenience.

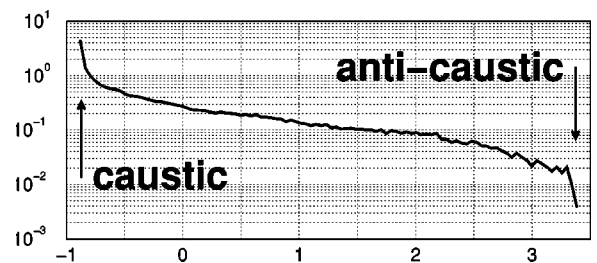


FIG. 3. The scaled classical profile $\hat{P}_{\text{cl}}(\cdot)$. One unit on the horizontal axis corresponds to energy difference $\delta E_{\text{cl}} \approx 0.38 * \delta x$. Note that $r=0$ implies $[E_n(x) - E_m(x_0)] > 0$. The caustic is located at $[E_n(x) - E_m(x_0)] = 0$, while the anticaustic is located at $[E_n(x) - E_m(x_0)] = 1.65 * x$. The “forbidden regions” are defined as those regions where $P_{\text{cl}}(r) = 0$. They are located to the left of the caustic and to the right of the anticaustic.

III. THE QUANTIZED HAMILTONIAN

Upon quantization we have a second dimensionless parameter \hbar . For obvious reasons we are considering a desymmetrized (1/8) well with Dirichlet boundary conditions on the lines $Q_1=0$, $Q_2=0$, and $Q_1=Q_2$. The matrix representation of $\mathcal{H}=\mathcal{H}(Q,P;x)$ in the basis, which is determined by $\mathcal{H}(Q,P;0)$, is very simple. The eigenstates ($n=1,2,3,\dots$) of the chaotic Hamiltonian $\mathcal{H}_0=\mathcal{H}(Q,P;1)$ has been found numerically.

The phase-space volume ($dQdP$ integral) which is enclosed by an energy surface $\mathcal{H}(Q,P;x)=E$, is given by a function $n=\Omega(E,x)$. It is convenient to measure phase-space volume in units of $(2\pi\hbar)^d$, where $d=2$ is the dimensionality of our system. Upon quantization the phase-space volume n corresponds to the level index ($n=1,2,3,\dots$). This is known as the Weyl law. It follows that $g(E)=\partial_E\Omega(E,x)$ corresponds to the density-of-states, and $\Delta=1/g(E)\propto\hbar^d$ is the mean level spacing.

In the following presentation we are going to assume the our interest is restricted to an energy window which is ‘‘classically small’’ but ‘‘quantum-mechanically large.’’ In the numerical analysis of our model Hamiltonian the energy window was $2.8<E<3.1$, where the classical motion is predominantly chaotic. The mean level spacing for $E\sim 3$ is given approximately by the formula $\Delta\approx 4.3*\hbar^2$. Our numerical analysis has been carried out for $\hbar=0.03$ and for $\hbar=0.015$. Smaller values of \hbar were beyond our numerical capabilities since the maximal matrix that we can handle is of size 5000×5000 .

The representation of $Q_1^2Q_2^2$, in the basis, which is determined by the chaotic Hamiltonian \mathcal{H}_0 , gives the matrix \mathbf{B} of Eq. (1). The banded matrix \mathbf{B} and the band profile are illustrated in Fig. 2. The band profile is implied by the semiclassical relation [1]:

$$|\mathbf{B}_{nm}|^2\approx\frac{\Delta}{2\pi\hbar}\tilde{C}\left(\frac{E_n-E_m}{\hbar}\right). \quad (6)$$

As we see from Fig. 2 the agreement with this formula is remarkable. For the bandwidth Eq. (6) implies that $\Delta_b=2\pi\hbar/\tau_{cl}$. It is common to define $b=\Delta_b/\Delta$.

IV. DEFINITION OF THE LOCAL DENSITY-OF-STATES PROFILE

The quantum eigenstates of the Hamiltonian $\mathcal{H}(Q,P;x)$ are $|n(x)\rangle$, and the ordered eigenenergies are $E_n(x)$. We are interested in the parametric kernel

$$P(n|m)=|\langle n(x)|m(x_0)\rangle|^2=\text{trace}(\rho_n\rho_m). \quad (7)$$

In the equation above $\rho_m(Q,P)$ and $\rho_n(Q,P)$ are the Wigner functions that correspond to the eigenstates $|m(x_0)\rangle$ and $|n(x)\rangle$, respectively. The trace stands for $dQdP/(2\pi\hbar)^d$ integration.

We can identify $P(n|m)$ as the local density of states (LDOS), by regarding it as a function of n , where m is considered to be a fixed reference state. An average of $P((m+r)|m)$ over several m states leads to the LDOS pro-

file $P(r)$. Alternatively, fixing n , the vector $P(n|m)$ describes the shape of the n th eigenstate in the \mathcal{H}_0 representation. By averaging $P(n|(n-r))$ over few eigenstates one obtains the average shape of the eigenstate (ASOE). The ASOE is just $P(-r)$. Thus the ASOE and the LDOS are given by the same function. One would have to be more careful with these definitions if \mathcal{H}_0 were integrable while \mathcal{H} is nonintegrable.

The kernel $P(n|m)$ gives the overlap between the n th eigenstate of \mathcal{H} and the m th eigenstate of \mathcal{H}_0 . For $\delta x=0$ we have simply $P(n|m)=\delta_{nm}$. For $\delta x>0$ the kernel develops a structure, which is described by the LDOS profile $P(r)$. If δx is very small then evidently $P(r)$ consists of Kronecker delta (at $r=0$) and tail regions ($|r|>0$). Later we are going to distinguish between first-order tail regions (FOTR's), and higher-order far-tail regions. As δx becomes larger a nonperturbative core region appears around $r=0$. Namely, the profile exhibits a bunch of states (rather than one) that share most of the probability. If δx becomes even larger, the distinction between core and tail regions become meaningless, and the LDOS profile becomes purely nonperturbative. We are going to explain that the nonperturbative profile reflects the underlying classical phase space structure.

V. THE CLASSICAL APPROXIMATION FOR THE LDOS

The classical approximation [9,5–7] for $P(n|m)$ follows naturally from the definition Eq. (7). It is obtained if we approximate $\rho_n(Q,P)$ by a microcanonical distribution that is supported by the energy surface $\mathcal{H}(Q,P;x)=E_n(x)$. Namely,

$$\begin{aligned} \rho_n(Q,P) &= \frac{1}{g(E)}\delta(\mathcal{H}(Q,P;x)-E_n(x)) \\ &= \delta(\Omega(\mathcal{H}(Q,P;x))-n) \end{aligned} \quad (8)$$

and a similar expression (with $x=x_0$) for $\rho_m(Q,P)$. In the classical limit n is the phase-space volume by which we label energy surfaces. Each energy surface n is associated with a microcanonical state $\rho_n(Q,P)$. The classical LDOS profile will be denoted by $P_{cl}(r)$. The δx regime, where the classical approximation $P(r)\approx P_{cl}(r)$ applies, will be discussed in a later section.

By definition, for $\delta x\ll\delta x_c^{cl}$ the deformed energy surfaces departs linearly from the $\delta x=0$ surfaces. As already stated in the Introduction, being in this classical linear regime is a fixed assumption of this paper. Now we want to explain the consequences of this assumption. One may consider these consequences as giving an operational definition for the classical linear regime. The dispersion (square root of the variance) of the classical profile in the classical linear regime is

$$\delta E_{cl}=\sqrt{C(0)}\times\delta x. \quad (9)$$

(This should be divided by Δ if we want the dispersion in proper r units. See Eq. (11) below.) For our model Hamiltonian, for energies $E\sim 3$, we have found that δE_{cl}

$\approx 0.38 * \delta x$. Equation (9) can be regarded as a special consequence of the following scaling relation, which we are going to derive below:

$$P_{\text{cl}}(r) = \frac{\Delta}{\sqrt{C(0)}\delta x} \hat{P}_{\text{cl}}\left(\frac{\Delta \cdot r}{\sqrt{C(0)}\delta x}\right). \quad (10)$$

The scaling function has already been defined in Eq. (5), and it is illustrated in Fig. 3. The classical profile $P_{\text{cl}}(r)$ is in general nonsymmetric, but it follows from Eq. (10) that it must be characterized by $\langle r \rangle = 0$. [By definition the scaling function of Eq. (5) gives zero average]. Another obvious feature is having sharp cutoffs, beyond which $P_{\text{cl}}(r) = 0$. The existence of these outer ‘‘classically forbidden’’ regions follows from the observation that for large enough r there is no longer classical overlap between the energy surfaces that correspond to $|m(x_0)\rangle$ and $|n(x)\rangle$, respectively.

The rest of this section is dedicated to technical clarifications of Eq. (10), and it can be skipped in first reading. The derivation is done in two steps. The first step is to establish a relation between $P_{\text{cl}}(r)$ and its trivially related version $P_{\text{E}}(\epsilon)$. The second step is to demonstrate that $P_{\text{E}}(\epsilon)$ is related to $P_{\text{F}}(\mathcal{F})$ of Eq. (5). It is also possible to make a one-step derivation that relates $P_{\text{cl}}(r)$ to $P_{\text{F}}(\mathcal{F})$, but we find the derivation below more physically appealing.

By differentiation of $n = \Omega(E, x)$, keeping n constant, we get the relation $\delta E = -F(x)\delta x$, where $F(x) = \partial_x \Omega(E, x)/g(E)$ is known as the (generalized) conservative force. Using the latter expression it is a straightforward exercise to prove that $F(x) = \langle \mathcal{F} \rangle \equiv F$. Alternatively, we can eliminate E from the relation $n = \Omega(E, x)$, and write the result as $E = E_n(x)$. Accordingly $F(x) = -[\partial E_n(x)/\partial x]$. Now we can write the following relation:

$$E_n(x) - E_m(x_0) = \frac{\partial E}{\partial x} \Big|_n \delta x + \frac{\partial E}{\partial n} \Big|_x (n - m),$$

which can be rewritten in the following form:

$$\epsilon = -F(x)\delta x + [1/g(E)]r. \quad (11)$$

Whenever we regard the kernel $P(n|m)$ as a function of $n - m$, we use the notation $P(r)$. But sometimes it is convenient to regard $P(n|m)$ as an energy distribution $P_{\text{E}}(\epsilon)$. Due to the change of variables (11) we have the following relation:

$$P(r) = \frac{1}{g(E)} P_{\text{E}}\left(\frac{1}{g(E)}r - F(x)\delta x\right). \quad (12)$$

The energy distribution $P_{\text{E}}(\epsilon)$ can be formally defined as follows:

$$P_{\text{E}}(\epsilon) = \sum_n P(n|m) \delta(\epsilon - [E_n(x) - E_m(x_0)]). \quad (13)$$

In the classical limit the summation over n should be interpreted as a dn integral. For $P(n|m)$ in the above expression

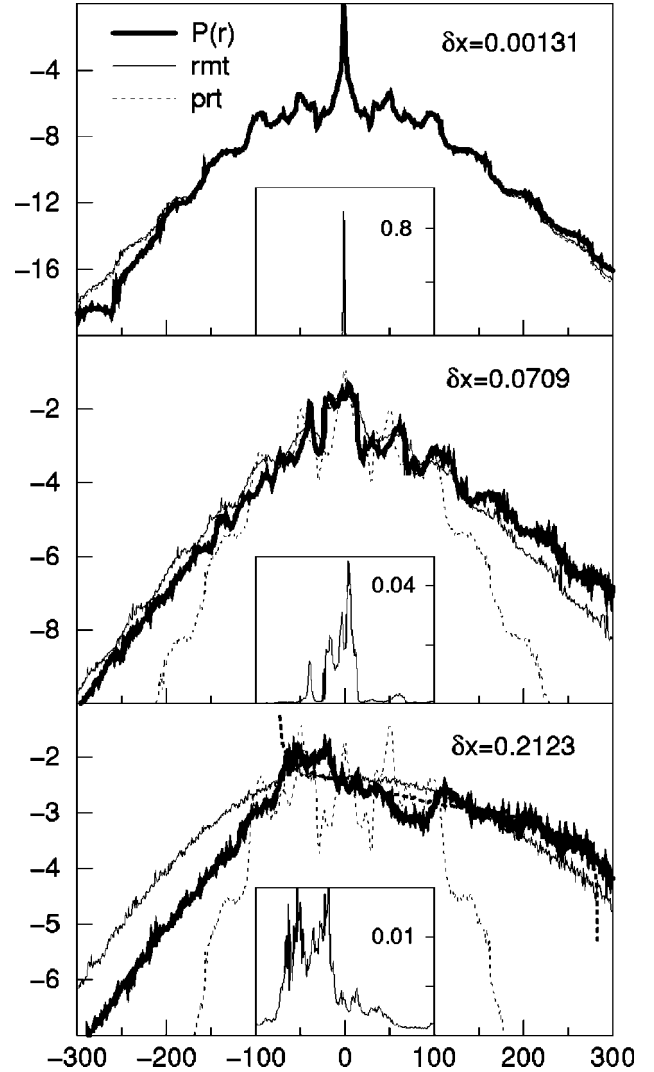


FIG. 4. The quantal profile $P(r)$ is compared with $P_{\text{prt}}(r)$ and with $P_{\text{RMT}}(r)$. We are using here the $\hbar = 0.015$ output. The insets are normal plots while the main figures are semilog plots. In the lower plot ($\delta x = 0.2123$) the classical LDOS profile $P_{\text{cl}}(r)$ is represented by a heavy dashed line.

we can substitute the definition [Eq. (7)] with ρ_n and ρ_m approximated as in Eq. (8). A straightforward manipulation leads to the result

$$\begin{aligned} P_{\text{E}}(\epsilon) &= \langle \delta(\epsilon - [\mathcal{H}(Q, P; x) - \mathcal{H}(Q, P; x_0)]) \rangle \\ &= \langle \delta(\epsilon + \delta x \mathcal{F}(t)) \rangle = \frac{1}{\delta x} P_{\text{F}}\left(-\frac{1}{\delta x} \epsilon\right). \end{aligned}$$

Together with Eqs. (5) and (12), we get Eq. (10) along with the implied special result (9).

VI. NUMERICAL DETERMINATION OF LDOS PROFILES

Given δx we can determine numerically the LDOS profile $P(r)$. Representative profiles are displayed in Fig. 4. For the purpose of further discussion we introduce the following definitions:

- (1) The classical LDOS profile $P_{\text{cl}}(r)$.
- (2) The quantum-mechanical LDOS profile $P(r)$.
- (3) The effective WBRM LDOS profile $P_{\text{RMT}}(r)$.
- (4) The first-order perturbative profile $P_{\text{prt}}(r)$.

We have already discussed the classical LDOS profile. Below we explain how we numerically determine the quantum-mechanical LDOS profiles $P(r)$ and $P_{\text{RMT}}(r)$, and we also define the profile $P_{\text{prt}}(r)$.

The numerical procedure for finding $P(r)$ is straightforward. For a given δx we have to diagonalize the matrix (1). The columns of the diagonalization matrix \mathbf{T}_{mn} are the eigenstates of the Hamiltonian, and by definition we have $P(n|m) = |\mathbf{T}_{mn}|^2$. Then $P(r)$ is computed by averaging over roughly 300 reference states that are located within the classically small energy window $2.8 < E < 3.1$. Figure 4 displays typical profiles.

The effective WBRM Hamiltonian is obtained by randomizing the signs of the off-diagonal elements in the \mathbf{B} matrix. For the effective WBRM Hamiltonian exactly the same procedure [as for $P(r)$] is applied leading to $P_{\text{RMT}}(r)$.

In order to analyze the structure of either $P(r)$ or $P_{\text{RMT}}(r)$, we have defined the first-order perturbative profile as follows:

$$P_{\text{prt}}(r) = \frac{\delta x^2 |\mathbf{B}_{nm}|^2}{\Gamma^2 + (E_n - E_m)^2}. \quad (14)$$

It is implicit in this definition that $(E_n - E_m)$ and $|\mathbf{B}_{nm}|^2$ should be regarded as a function of r . The $r=0$ value of the band profile should be redefined by an interpolation. The parameter $\Gamma \equiv b_0 \Delta$ is determined (for a given δx) such that the $P_{\text{prt}}(r)$ has a unit normalization. Note that Wigner's Lorentzian would be obtained if the band profile were flat.

VII. REGION ANALYSIS FOR THE QUANTAL LOCAL DENSITY OF STATES

By comparing $P(r)$ to $P_{\text{prt}}(r)$ as in Fig. 4, we can determine² the range $b_1[\text{left}] < r < b_1[\text{right}]$, where $P_{\text{prt}}(r)$ is a reasonable approximation for $P(r)$. Loosely speaking (avoiding the distinction between the ‘‘left’’ and the ‘‘right’’ sides of the profile) we shall say that $P_{\text{prt}}(r)$ is a reasonable approximation for $|r| < b_1$. The core is defined as the region $|r| < b_0$. The FOTR's are $b_0 < |r| < b_1$. The far-tail regions are $|r| > b_1$.

The results of this region analysis are summarized by Fig. 5. In the following sections we are going to present a de-

²The determination of b_1 has been done using the following numerical procedure. We define relative error function $\text{RE}(r) = (P - P_{\text{prt}})/(P + P_{\text{prt}})$ and then cumulative error function $\text{CRE}(r) = |\sum_0^r \text{RE}(r')|$. Note that by this definition ‘‘positive’’ relative error can be compensated by ‘‘negative’’ relative error. As we go away from $r=0$, the function $\text{CRE}(r)$ fluctuates, and later shoots up. The regime $|r| < b_1$ has been determined by the condition $\text{CRE}(r) < \text{threshold}$. The threshold has been determined using an adaptively procedure.

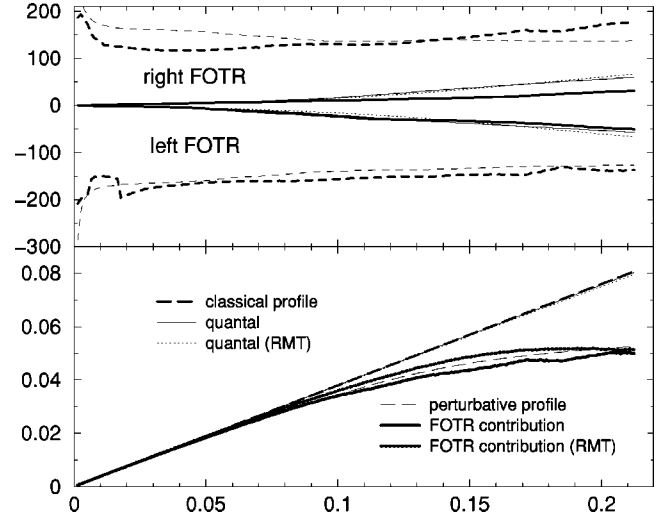


FIG. 5. The results of region analysis. The common horizontal axis is δx . The *upper figure* presents the r boundaries as a function of δx . The dotted lines $\pm b_0$ define the core region ($|r| < b_0$). The solid lines define the r region in which 50% of the probability is concentrated. The dashed lines are $b_1[\text{left}]$ and $b_1[\text{right}]$. The FOTR's are the regions where $b_0 < |r| < b_1$. The light-solid lines and the light-dashed lines are for the effective WBRM model. The *lower figure* displays the dependence of δE_{cl} , δE_{qm} , and δE_{prt} on δx . The quantal and the classical results are almost indistinguishable, whereas δE_{prt} approaches saturation. The contribution of the FOTR's to δE_{qm} is also displayed.

tailed discussion of this analysis. For the convenience of the reader we summarize: (1) $b_0 =$ border of the core region; (2) $b_1 =$ border of the FOTR. Having $b_0 \ll 1$ implies a standard perturbative structure. Having $1 \ll b_0 \ll b_1$ implies that we have a well-developed core-tail structure. Having $b_0 \sim b_1$ implies a purely nonperturbative structure. In the latter case the distinction between core and tail regions become meaningless.

VIII. THE STANDARD PERTURBATIVE REGIME

The standard perturbative regime $\delta x \ll \delta x_c^{\text{qm}}$ is defined by the requirement $b_0(\delta x) \ll 1$. This condition implies that $P(n|m) \sim \delta_{nm}$. For numerical purpose it is convenient to define δx_c^{qm} as the value of δx for which $P(r=0) \approx 0.5$. The theoretical considerations of Ref. [5] imply that $\delta x_c^{\text{qm}} \propto \hbar^{(1+d)/2}$. The prefactor is a classical quantity whose precise value depends on the operational definition of δx_c^{qm} . With the operational definition given above we have extracted the result $\delta x_c^{\text{qm}} \approx 3.8 * \hbar^{3/2}$.

In the standard perturbative regime we can write schematically

$$P(n|m) \approx \delta_{nm} + \text{Tail}. \quad (15)$$

The ‘‘Tail’’ is composed of FOTR's and far-tail regions. The former are given by Eq. (14), while the latter are determined by higher orders of perturbation theory. Note that for the

standard WBRM we have by construction $b_1 \equiv b$, and more generally n th order perturbation theory becomes essential for $(n-1) \times b < |r| < n \times b$. In case of our physical Hamiltonian, as well as for the associated *effective* WBRM model, the boundary b_1 is δx dependent.

By comparing $P(r)$ with $P_{\text{RMT}}(r)$ we can see that RMT cannot be trusted for the analysis of the far tails, because system-specific interference phenomena becomes important there. Namely, the RMT profile $P_{\text{RMT}}(r)$ is almost indistinguishable from $P_{\text{prt}}(r)$. In contrast to that, the far tails of $P(r)$ are dominated by either destructive interference (left tail), or by constructive interference (right tail).

IX. THE CORE-TAIL REGIME

The core-tail regime $\delta x_c^{\text{qm}} \ll \delta x \ll \delta x_{\text{prt}}$ is defined by the requirement $1 \ll b_0 \ll b_1$. The theoretical considerations of Ref. [5] imply that $\delta x_{\text{prt}} \propto \hbar$. The prefactor is a classical quantity whose precise value depends on the operational definition of δx_{prt} . In our numerical analysis we have defined δx_{prt} as the δx for which the contribution of the FOTR's to the variance becomes less than 80%. With this operational definition we have extracted (using the lower subplot of Fig. 5) the result $\delta x_{\text{prt}} \approx 5.3 * \hbar$.

In the core-tail regime we can write schematically

$$P(n|m) \approx \text{Core} + \text{Tail}. \quad (16)$$

Disregarding the far-tail regions, the large-scale behavior of $P(r)$ can be approximated by that of $P_{\text{prt}}(r)$. As in the standard perturbative regime one observes that the far tails are dominated by either destructive interference (left tail), or by constructive interference (right tail).

The core is a nonperturbative region. It means, that unlike the far tail, it cannot be obtained from any finite-order perturbation theory. Once the core appears, the validity of first-order perturbation theory becomes a nontrivial matter. In Ref. [5] a nonrigorous argument is suggested in order to support the claim that, disregarding the smoothing effect, the local mixing of neighboring levels does not affect the growth of the tail. An important ingredient in this argumentation is the (self-consistent) assumption that most of the probability is well-contained in the core region. Indeed the analysis, which is presented in Fig. 5, is in agreement with this assumption.

The observation that the local mixing of neighboring levels does not affect the growth of the tail, implies that the tail grows as δx^2 and not like say δx . (The latter type of dependence is implied by an oversimplified argumentation.) Having indeed δx^2 behavior is implied by observing that $P(r) \approx P_{\text{prt}}(r)$ for the FOTR's.

Finally, it should be emphasized that the local mixing of levels on the small scale b_0 is not reflected by Eq. (14). In particular, one should not expect Eq. (14) to be literally valid within the core region ($|r| < b_0$).

X. THE NONPERTURBATIVE REGIME

In the nonperturbative regime ($\delta x \gg \delta x_{\text{prt}}$) one may say that the core spills over the FOTR's and therefore $P(n|m)$

becomes purely nonperturbative. As an example for nonperturbative profile let us consider the lower plot of Fig. 4, corresponding to $\delta x = 0.2123$. We see that there is poor resemblance between $P(r)$ and $P_{\text{prt}}(r)$. The LDOS profile $P(r)$ no longer contains a predominant FOTR's. This claim can be quantified using the analysis in Fig. 5. The lower figure there displays the FOTR contribution to the dispersion. For $\delta x > \delta x_{\text{prt}}$ the dispersion is no longer determined by the FOTR contribution.

The complete disappearance of FOTR's is guaranteed only for $\delta x \gg \delta x_{\text{prt}}$. Evidently, for $\delta x \gg \delta x_{\text{prt}}$ the FOTR's must disappear, because $P(r)$ goes on expanding, while $P_{\text{prt}}(r)$ saturates. This is not captured by our numerics, since for $\hbar = 0.015$, we cannot satisfy the strong inequality $\delta x \gg \delta x_{\text{prt}}$, and have a classically small δx at the same time.

XI. THE SEMICLASSICAL REGIME

Looking back at the lower plot of Fig. 4, we see that detailed QCC with the classical profile (represented by heavy-dashed line) starts to develop. The right far tail contains a component where $P(r)$ and $P_{\text{cl}}(r)$ are indistinguishable. This detailed QCC obviously does not hold for the RMT profile.

Being in the nonperturbative regime does not imply detailed QCC [10,5,6]. Detailed QCC means that $P(r)$ can be approximated by $P_{\text{cl}}(r)$. Having $\delta x \gg \delta x_{\text{prt}}$ is a necessary rather than sufficient condition for detailed QCC. A sufficient condition for detailed QCC is $\delta x \gg \delta x_{\text{SC}}$. The parametric scale δx_{SC} is defined in Ref. [5], and for our system we can obtain the (theoretical) rough estimate $\delta x_{\text{SC}} \approx 4 * \hbar^{2/3}$.

In our numerical study we could not make \hbar small enough such that $\delta x_{\text{SC}} \ll \delta x_c^{\text{cl}}$. Therefore, the lower profile in Fig. 4 is neither reasonably approximated by $P_{\text{prt}}(r)$, nor by $P_{\text{cl}}(r)$. However, we have verified (by comparing the $\hbar = 0.03$ output to the $\hbar = 0.015$ output) that detailed QCC between $P(r)$ and $P_{\text{cl}}(r)$ is easily improved by making \hbar smaller. Comparing $P(r)$ to $P_{\text{cl}}(r)$ on the one hand, and $P_{\text{RMT}}(r)$ to $P_{\text{cl}}(r)$ on the other hand, leaves no doubt regarding the manifestation of underlying classical structures.

Using a phase-space picture [5,6] it is evident that larger δx leads to better QCC. The WBRM model does not have a classical limit, and one finds a quite different scenario [3]. For large enough δx the eigenstates of Eq.(1) become Anderson localized. This localization shows up in the ASOE *provided* the eigenstates are properly centered prior to averaging. In the (nonaveraged) LDOS, localization manifests itself as sparsity, and therefore the various moments of the LDOS profile are not affected. This latter remark should be kept in mind while reading the next section.

XII. RESTRICTED QCC

It is important to distinguish between detailed QCC and restricted QCC. Let us denote the dispersion of the quantal LDOS profile by δE_{qm} . The corresponding classical quantity is given by Eq. (9). The two types of QCC are defined as follows:

- (1) Detailed QCC means $P(r) \approx P_{\text{cl}}(r)$.

(2) Restricted QCC means $\delta E_{\text{qm}} \approx \delta E_{\text{cl}}$.

Obviously restricted QCC is a trivial consequence of detailed QCC, but the converse is not true. It turns out that restricted QCC is much more robust than detailed QCC. In Fig. 5 we see that the dispersion δE_{qm} of either $P(r)$ or $P_{\text{RMT}}(r)$ is almost indistinguishable from δE_{cl} . This is quite remarkable because the corresponding LDOS profiles (quantal versus classical) are very different!

It is important to realize that restricted QCC is implied by first-order perturbation theory. If we use Eq. (14) and take into account the FOTR dominance, which is implied by $\delta x \ll \delta x_{\text{prt}}$, then we get simply

$$\delta E_{\text{qm}} = \sum_n P(n|m)(E_n - E_m)^2 = \delta x^2 \sum_n ' |\mathbf{B}_{nm}|^2, \quad (17)$$

where prime indicates omission of the $n = m$ term. Using Eq. (6) one realizes that this result is in complete agreement with Eq. (9). In contrast to that, higher moments of the perturbative profile are vanishingly small compared with the corresponding classical result. The latter fact is just a reflection of the absence of detailed QCC.

One may wonder what happens with Eq. (17) if we try to do a better work, taking into account the core width, as well as higher-order far-tails contributions. One may think that

Eq. (17) is only the lowest-order approximation, which would imply that restricted QCC should become worse as δx grows. However, the latter speculation turns out to be wrong.

We already saw that restricted QCC is implied on the one hand (for small δx) by first-order perturbation theory, and on the other hand (for large δx) by detailed QCC. Now we would like to argue that restricted QCC holds in general. It simply follows from the observation that δE_{qm} is determined just by the band profile. The proof is very simple [3]. The variance of $P(n|m)$ is determined by the first two moments of the Hamiltonian in the unperturbed basis. Namely,

$$\begin{aligned} \delta E_{\text{qm}}^2 &= \langle m | \mathcal{H}^2 | m \rangle - \langle m | \mathcal{H} | m \rangle^2 \\ &= \delta x^2 (\langle m | \mathbf{B}^2 | m \rangle - \langle m | \mathbf{B} | m \rangle^2). \end{aligned}$$

Thus, we get the same result as in first-order perturbation theory without invoking any special assumptions regarding the nature of the profile. Having δE_{qm} that is determined only by the band profile, is the reason for restricted QCC, and is also the reason why restricted QCC is not sensitive to the RMT assumption.

ACKNOWLEDGMENTS

The authors thank Felix Izrailev for suggesting to study model (2). We also thank ITAMP for their support.

-
- [1] M. Feingold and A. Peres, *Phys. Rev. A* **34**, 591 (1986); M. Feingold, D. Leitner, and M. Wilkinson, *Phys. Rev. Lett.* **66**, 986 (1991); M. Wilkinson, M. Feingold, and D. Leitner, *J. Phys. A* **24**, 175 (1991); M. Feingold, A. Gioletta, F. M. Izrailev, and L. Molinari, *Phys. Rev. Lett.* **70**, 2936 (1993).
- [2] E. Wigner, *Ann. Math.* **62**, 548 (1955); **65**, 203 (1957).
- [3] G. Casati, B. V. Chirikov, I. Guarneri, and F. M. Izrailev, *Phys. Rev. E* **48**, R1613 (1993); *Phys. Lett. A* **223**, 430 (1996); V. V. Flambaum, A. A. Gribakina, G. F. Gribakin, and M. G. Kozlov, *Phys. Rev. A* **50**, 267 (1994).
- [4] Y. V. Fyodorov, O. A. Chubykalo, F. M. Izrailev, and G. Casati, *Phys. Rev. Lett.* **76**, 1603 (1996).
- [5] D. Cohen, *Ann. Phys. (N.Y.)* **283**, 175 (2000).
- [6] D. Cohen, in *Proceedings of the International School of Physics "Enrico Fermi," Course CXLIII, New Directions in Quantum Chaos*, edited by G. Casati, I. Guarneri, and U. Smilansky (IOS Press, Amsterdam, 2000).
- [7] D. Cohen and E. J. Heller, *Phys. Rev. Lett.* **84**, 2841 (2000).
- [8] In a later work regarding "Parametric evolution for a deformed cavity" [D. Cohen, A. Barnett, and E. J. Heller, *Phys. Rev. E* (to be published); nlin.CD/0008040], further study of the various parametric regimes is introduced. In our present paper the emphasis is on generic features of parametric evolution, while in nlin.CD/0008040 the emphasis is on nongeneric features, which have been discussed in Ref. [7].
- [9] F. Borgonovi, I. Guarneri, and F. M. Izrailev, *Phys. Rev. E* **57**, 5291 (1998); L. Benet, F. M. Izrailev, T. H. Seligman, and A. Suarez-Moreno, *Phys. Lett. A* **277**, 87 (2000).
- [10] D. Cohen, *Phys. Rev. Lett.* **82**, 4951 (1999).
- [11] D. Cohen, F. M. Izrailev, and T. Kottos, *Phys. Rev. Lett.* **84**, 2052 (2000).